Journal of Material Science and Mechanical Engineering (JMSME)
p-ISSN: 2393-9095; e-ISSN: 2393-9109; Volume 11, Issue 1; January-March, 2024, pp. 10-16

http://www.krishisanskriti.org/Publication.html

Solid Particle Erosive behaviour of Hypo-eutectoid and Hyper-eutectoid Bainitic Steel

P. C. Mani[1], R. Manna[2] and A. P. Harsha[3]

[1]Assistant Professor, Department of Mechanical Engineering, IIT (BHU) Varanasi
[2]Associate Professor, Department of Metallurgical Engineering, IIT (BHU) Varanasi
[3]Professor, Department of Mechanical Engineering, IIT (BHU) Varanasi
E-mail: [1]pcmani.mec@iitbhu.ac.in, [2]rmanna.met@iitbhu.ac.in, [3]apharsha.mec@iitbhu.ac.in

Abstract—*Solid particle erosive behaviour of hypo-eutectoid and hyper-eutectoid bainitic steel was reported in the present study, where 0.69C hypo-eutectoid and 1.17C hyper-eutectoid steel were austenitized at 900°C and 800°C followed by austempering at 250°C temperature for bainitic transformation. Microstructure was characterized by optical microscopy and hardness was measured. Erosion resistance of hypo-eutectoid and hyper-eutectoid bainitic steel were compared by subjecting them to erosive wear at varied impact angles ranging from 15° to 90° with varying velocities from 40m/s to 90m/s and Steady State Erosion Rate (SSER) was determined using 50 µm sharp alumina particles as an erodent. The erosion behaviour was correlated with the erosion power law model ($E=k*v^n$) and obtained the velocity exponent (n) for respective impact velocities. The average value of the velocity exponent (n) was 2.01 for hypo-eutectoid bainitic steel and 2.39 for hyper-eutectoid bainitic steel, which proved the ductile erosive behaviour of aforesaid steels. The SSER of hypo-eutectoid bainitic steel was maximum at 30° impact angle for all velocities while for hyper-eutectoid bainitic steels, it was maximum at 60° impact angle for 40-60 m/s and 30° impact angle for 90m/s. The SSER of hypo-eutectoid and hyper-eutectoid bainitic steel was minimum at 90° impact angle for all velocities. Scanning Electron Microscopy (SEM) analysis of eroded surfaces showed different erosion mechanisms. SEM analysis of eroded samples was examined to know the different erosion mechanisms like ploughing, cutting, pit formation, etc. At low impact angles erosion of bainitic steel was observed ploughing with lip formation but ploughing decreases with increasing hardness while at high impact angles cutting, crack formation with pits, crater formation, and splashing of materials as well as embedding of erodent was observed. Further, it was observed that cutting, embedding, and crater formation with a splash were increased with increasing hardness.*

1. INTRODUCTION

Solid particle erosion [1, 8] involves material removal from surfaces due to the continuous impact of hard, angular particles at high velocities. It poses a significant concern in engineering applications like valves, hydraulic systems, pipelines, aeronautical components, hydraulic pumps, and turbine blades. Surface erosion has garnered attention, leading to extensive studies on the impact of variables such as particle properties, material characteristics, and impact conditions. Factors like shape, size, hardness, impact angle, and velocity of the erodent, as well as target material properties, influence erosion behaviour [2-8]. The impact velocity of erodent particles plays a crucial role, and the power law model is commonly used to correlate erosion rate with impact velocity

$$E = k*v^n \quad (1)$$

In equation (1), $\boldsymbol{E}$ represents the steady-state erosion rate (SSER), $\boldsymbol{k}$ is an empirical constant, $\boldsymbol{v}$ denotes the impact velocity of the erodent, and $\boldsymbol{n}$ stands for the velocity exponent [8, 33]. Previous studies by researchers such as Tilly, Finnie, Sundararajan, and Roy have extensively investigated the relationship between erosion rate and various variables in solid particle erosion of metals and alloys [1-4]. The erosion behaviour is influenced by factors including erosion conditions and erodent characteristics (shape, size, hardness) [3, 5-11]. Early research by Rosenberg on wear resistance in carbon steels highlighted that lamellar pearlite demonstrated superior wear resistance, while granular pearlite and the presence of free ferrite or free cementite in spheroidal form were detrimental [12]. Empirical studies have shown a power law relationship between erosion rate and velocity in metallic materials [3, 13-18]. The increase in erosion rate with velocity is attributed to the heightened kinetic energy of the erodent, resulting in more effective damage to the metal surface and impacting additional target material attributes [19–21, 32].

In this study, the solid particle erosive behaviour of hypo-eutectoid and hyper-eutectoid bainitic steel against alumina (Al_2O_3) was investigated. The 0.69C hypo-eutectoid and 1.17C hyper-eutectoid steel underwent austenitization and austempering for bainitic transformation. Microstructural analysis utilized optical microscopy, SEM secondary electron imaging, and XRD analysis. Erosive wear tests, conducted at velocities of 40-90 m/s and impact angles of 15°-90° using 50 µm sharp alumina particles, determined steady-state erosion rates (SSER). The erosion behaviour was correlated using the power law model, identifying the velocity exponent for different materials. Scanning electron microscopy analysis examined eroded samples to understand various erosion mechanisms.

2. EXPERIMENTAL DETAILS

Selection of Materials

Heat-treated 0.69C hypo-eutectoid and 1.17C hyper-eutectoid steel samples underwent erosion testing with alumina particles. The as-received 0.69C and 1.17C steel samples were austenitized at 900°C and 800°C, respectively, followed by austempering at 250°C for bainitic transformation. This treatment was specifically conducted for room temperature erosion studies against alumina (Al_2O_3) particles. Refer to Table 1 for steel chemical composition and Table 2 for modulus of elasticity and hardness values.

Table 1: Chemical composition of 0.69C hypo-eutectoid and 1.17C hyper-eutectoid steel

Elements	0.69C hypo-eutectoid steel	1.17C hyper-eutectoid steel
C	0.686	1.17
Si	0.129	0.267
Mn	0.693	0.446
P	0.0298	0.0280
S	0.0751	0.0136
Cr	0.162	0.197
Bi	-	0.198

3. MATERIALS AND METHODS

The heat-treated 0.69C hypo-eutectoid and 1.17C hyper-eutectoid steel underwent bainitic transformation through a heat treatment process, with phases identified and quantified using XRD. Erosion tests were conducted under various parameters to assess the erosive behaviour of the heat-treated steel. The obtained erosion data were correlated with the erosion power law model, determining velocity exponent values for both hypo-eutectoid and hyper-eutectoid steel. A comparison of erosion resistance was made between 0.69C hypo-eutectoid and 1.17C hyper-eutectoid bainitic steel. The heat-treated steel was exposed to erosive wear at velocities of 40m/s, 60m/s, and 90m/s, with impact angles of 15°, 30°, 60°, and 90°, using 50µm alumina particles as the erodent, and the steady-state erosion rate was measured.

The sample holder of the erosion testing machine has two different types of sample dimensions:

Dimension 1: 25 x 25 x 5 (mm^3)

Dimension 2: 25 x 20 x 5 (mm^3)

For erosion testing, 12 samples were made for hypo-eutectoid / hyper-eutectoid bainitic samples. Out of these 12 samples were utilised for the erosion testing: 6 samples were of dimension 1 and 6 samples were of dimension 2.

Table 2: Modulus of Elasticity and Hardness of 0.69C hypo-eutectoid and 1.17C hyper-eutectoid steel

Modulus of Elasticity (E) and Hardness (HV)			
Material	**Notation**	**E (GPa)**	**HV (Vickers)**
0.69C	0.69C (as received)	262.019	406.846
	0.69C bainite	270.392	513.017
1.17C	1.17C (as received)	261.518	405.568
	1.17C bainite	276.883	594.307

4. PHASE/MICROSTRUCTURAL ANALYSIS

1. As received 0.69C Steel

In Figure 1(a and c), the microstructure reveals the formation of pro-eutectoid ferrite (lighter phase) and pearlite (darker phase). The pearlite, consisting of alternating layers of ferrite and cementite (Fe_3C), appears coarse at 100x magnification. The pro-eutectoid ferrite takes on a polygonal shape between the pearlitic phase, with the pearlite being the predominant phase observed.

2. As received 1.17C Steel

In Figure 1(b and d), the microstructure displays pro-eutectoid cementite (lighter phase) and pearlite (darker phase). Cementite (Fe_3C) forms along the grain boundary in a continuous manner. The coarse formation of pearlite is easily distinguishable at 100x magnification.

3. Bainitic Steel (0.69C /1.17C)

In Figures 1(e and g) and Figures 1(f and h), the microstructure suggests the presence of 0.69 C hypo-eutectoid bainite and 1.17 C hyper-eutectoid bainite, respectively. Both exhibit a leaf-like inter-lamellar structure resembling parallel plates. The darker phase corresponds to α-ferrite, while the lighter phase is cementite (Fe_3C). XRD analysis in Figures 2(a) and 2(b) provides detailed insights into α-ferrite and cementite for quantitative phase analysis of the bainitic steel.

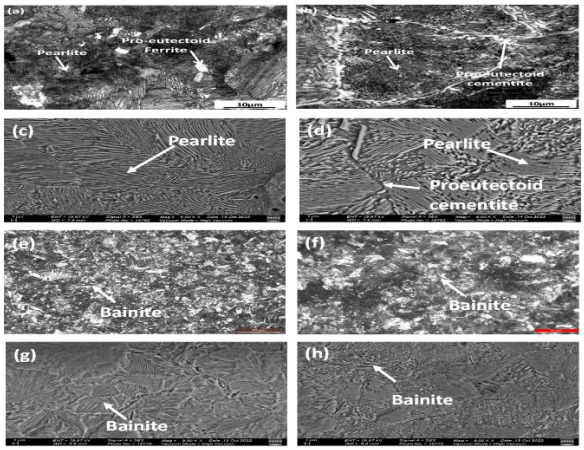

Figure 1: (a & c) optical/SEM micrograph of as received 0.69 C, (b & d) optical/SEM micrograph of as received 1.17 C, (e & g) optical/SEM micrograph of bainite 0.69 C, and (f & h) optical/SEM micrograph of bainite 1.17 C

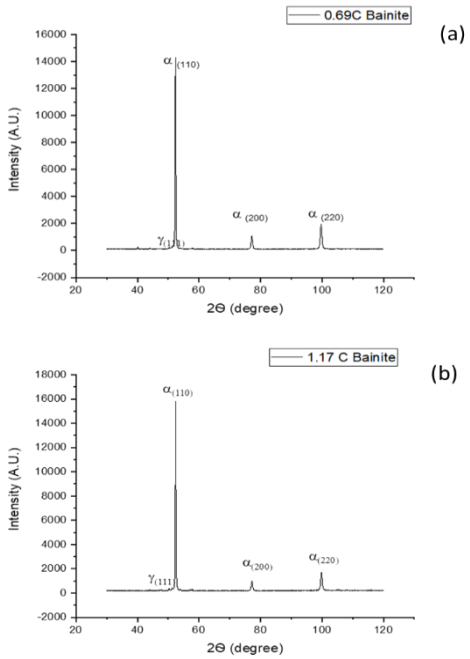

Figure 2: XRD spectra of (a) 0.69% carbon bainitic steel and (b) 1.17% carbon bainitic steel

5. ERODENT FOR EROSION TEST

The Alumina sand, consisting of fine, lightweight flakes with hygroscopic properties prone to clumping due to moisture absorption, underwent sieving and heating to 150-200 °C for 2 hours before use to eliminate trapped moisture. The moisture-free erodent was stored in a beaker and placed in a dry storage container with relative humidity below 20%, utilizing desiccators with silica gel powder. The prepared alumina was then introduced into the erosion tester for testing (Figure 3).

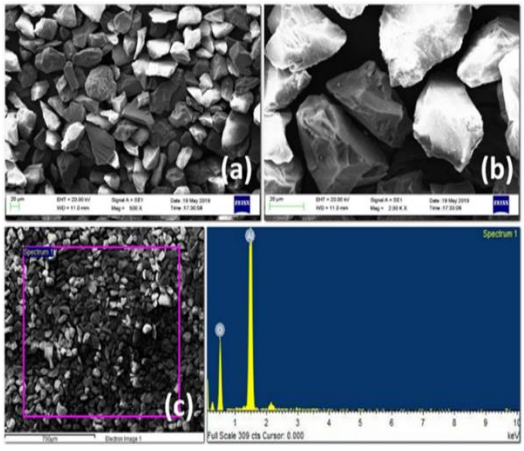

Figure 3: SEM micrograph of alumina sand particles at (a) 500xand (b) 2000x magnification and (c) EDS spectrum of alumina sand particles

Air Jet Erosion Test

4. Air Jet Erosion Test Rig

The DUCOM TR–471-400 air jet erosion tester (Figure 4) evaluated material erosion resistance through repeated impact erosion following ASTM G76. The test uses a smaller diameter nozzle to deliver an air stream with controlled velocity and erodent density. Erodent flux is regulated by a discharge unit, enabling adjustable discharge rates (0.5 to 10 g/min) by modifying wheel rotation speed. The pressurized air and erodent mixture exits through a smaller diameter nozzle, gaining velocity due to the diameter difference. Uniform flow without turbulence is maintained by a large length-to-diameter ratio in the nozzle. After impacting the specimen, the erodent loses kinetic energy, falling into the bottom chamber, and is manually removed post-testing. Further details on the air jet erosion tester parameters can be found in Table 3.

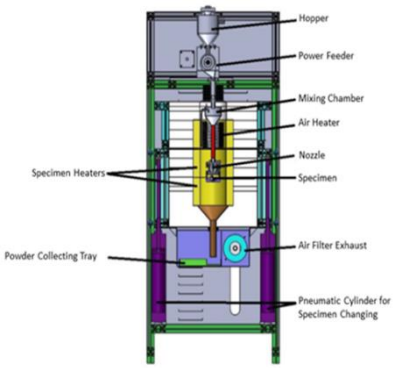

Figure 4: Schematic diagram of air jet erosion tester, courtesy DUCOM, India [34]

Table 3. Erosive Test Parameters

Parameters	Value
Nozzle Diameter and Material	$\phi 1.5 \pm 0.075$ mm made of 99.9% pure Alumina.
Erodent	50 µm diameter Alumina Sand
Erodent Shape	Irregular, sharp
Temperature	Room Temperature
Nozzle to Sample Distance	10 mm
Test Duration	10 minutes
Erodent Discharge Rate (Frequency of discharge wheel)	5.4 g/min (12 Hz)
Air Velocities	40 m/s, 60 m/s, 90 m/s
Erosion Angles (Specimen Dimension)	15° (25 x 20 x 5 mm^3), 30° (25 x 20 x 5 mm^3), 60° (25 x 25 x 5 mm^3), and 90° (25 x 25 x 5 mm^3).

6. RESULTS AND DISCUSSIONS

Erosion Rate and Steady State Erosion Rate

Plain carbon steel, chosen for its practical significance and versatility in heat treatment, facilitated a wide range of mechanical property variations. The study generated graphs

correlating incremental erosion rates with cumulative erodent weight for each test sample. Findings revealed that incremental erosion rates stabilize with increasing cumulative erodent weight, establishing the steady-state erosion rate (SSER) for each sample. Figures 5(a, b, c) and 6(a, b, c) illustrate erosion rates for 0.69 bainitic and 1.17C bainitic steel samples, respectively, plotted against cumulative weight at different impingement angles (15^{O} to 90^{O}) and impact velocities (40 m/s to 90 m/s). Initial erosion rates increase with accumulating alumina particles, stabilizing as micro-cutting initiates on the steel surface. Cumulative weight for reaching a steady state ranged from 100g to 400g for 0.69C bainitic steel and from 100g to 150g for 1.17C bainitic steel, irrespective of the impact angle. The SSER of hypo-eutectoid bainitic steel was maximum at 30° impact angle for all velocities while for hyper-eutectoid bainitic steels, it was maximum at 60° impact angle for 30-60 m/s and 30° impact angle for 90m/s. The SSER of hypo-eutectoid and hyper-eutectoid bainitic steel was minimum at 90° impact angle for all velocities. Table 4 and Table 5 present SSER values for 0.69 C bainitic/1.17 C bainitic steel. Consistent with previous research on erosion behaviour in engineering materials [4, 8, 22-25], this study aligns with observations on the significant impact of embedding erosive particles on the sample surface, resulting in substantial weight gain due to continuous embedded layers. Kosel et al.'s work [30, 31] on alumina erosion on nickel demonstrated a continuous composite surface layer with alumina particle fragments mixed with metal debris, revealing re-fragmentation upon further erodent particle impact

Table 4: Steady-state erosion rate of 0.69 C

Angle Velocity	15º	30º	60º	90º
40 m/s	1.12E-04	1.33E-04	9.04E-05	6.56E-05
60 m/s	2.21E-04	2.67E-04	2.63E-04	1.64E-04
90 m/s	5.14E-04	5.29E-04	4.91E-04	4.51E-04

Table 5: Steady-state erosion rate of 1.17 C

Angle Velocity	15º	30º	60º	90º
40 m/s	3.69E-05	3.81E-05	4.19E-05	3.18E-05
60 m/s	1.29E-04	1.30E-04	1.35E-04	8.61E-05
90 m/s	2.79E-04	2.83E-04	2.74E-04	2.02E-04

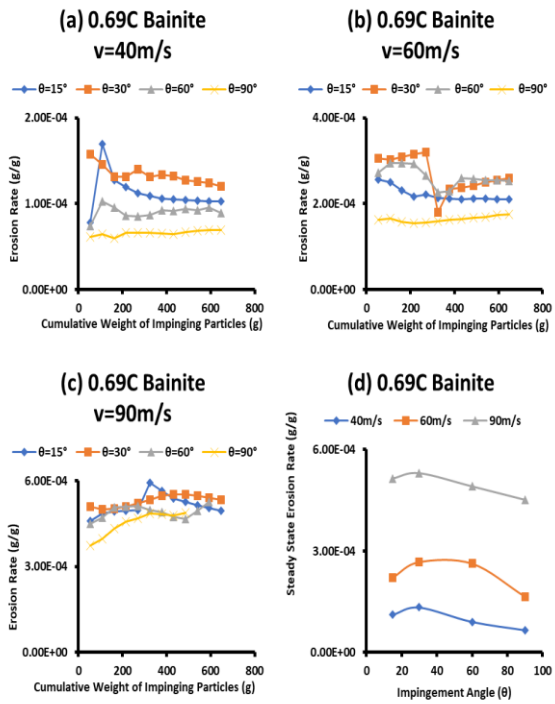

Figure 5: Variation of incremental erosion rate of 0.69 wt% C Bainitic steel with a cumulative weight of impinging particles at impact velocities of (a) 40m/s (b) 60m/s and (c) 90m/s (d) Comparison of SSER vs Impact Angle

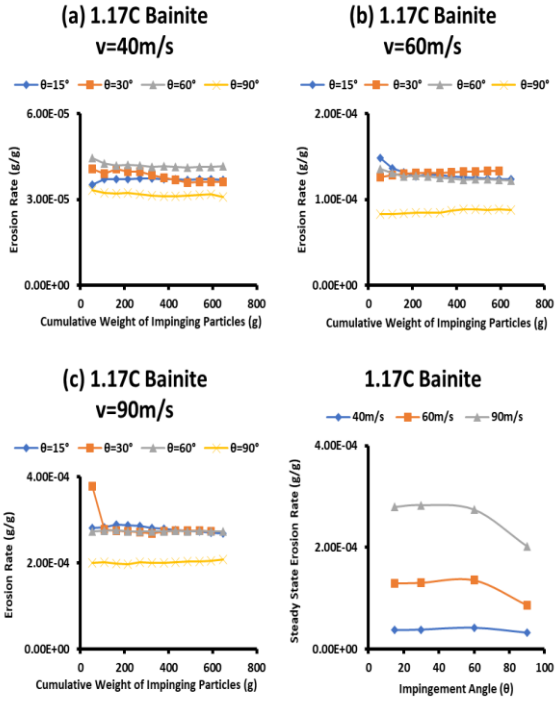

Figure 6: Variation of incremental erosion rate of 1.17wt% C Bainitic steel with a cumulative weight of impinging particles at impact velocities of (a) 40m/s (b) 60m/s and (c) 90m/s (d) Comparison of SSER vs Impact Angle.

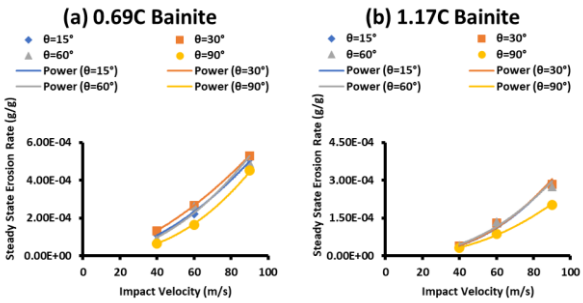

Figure 7: Variation of SSER of (a) 0.69 wt% C steel (b) 1.17wt% C steel l as a function of impact velocity

Velocity Exponent (n) Values

The velocity exponents (described by equation (1)) corresponding to various microstructures and velocities were computed and documented in Table 6. The calculation involved fitting the SSER graph against impact velocity (refer to Figure 7) using the power equation within Microsoft Excel software. To assess the fitness of the model, the R^2 value was determined. According to prior literature, materials exhibiting $2 < n < 3$ demonstrate ductile behavior, while those with $3 < n < 5$ exhibit brittle erosive behavior [8, 33]. Therefore, the ductile erosive behaviors of the Bainitic steel samples are reflected in the values of n = 2.01 for 0.69 C bainitic Steel and n = 2.39 for 1.17 C bainitic Steel. The R^2 value exceeds 0.9786 for all materials, indicating a strong fit of the data points. It is noteworthy that no direct correlation was observed between k, n, and VHN.

Table 6: k, n, and R^2 values of different materials

Material	Impact Angle	k	n	$n_{avg.}$	R^2
0.69 C Bainitic Steel	15º	1×10^{-7}	1.8834	2.01	0.9975
	30º	3×10^{-7}	1.6999		1.0000
	60º	4×10^{-8}	2.0859		0.9786
	90º	1×10^{-8}	2.3786		0.9995
1.17 C Bainitic Steel	15º	4×10^{-9}	2.4958	2.39	0.9842
	30º	4×10^{-9}	2.4722		0.9858
	60º	9×10^{-9}	2.3159		0.9820
	90º	7×10^{-9}	2.2784		0.9985

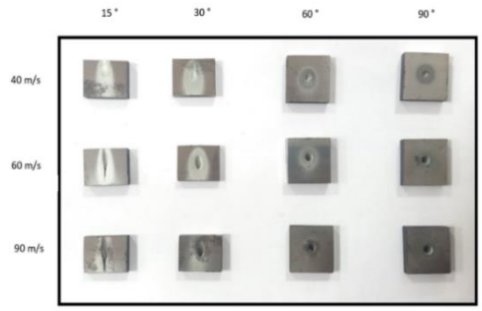

Figure 8: Eroded samples at different impact angles and velocities

Worn Surface Analysis Using SEM

In Figure 8, eroded samples from air jet erosion tests on bainitic steel exhibit distinct patterns based on impact angles and velocities. The heavily eroded lower right-hand corner results from higher impact angles and velocities, while the lightly eroded left-hand top corner is attributed to lower impact angles and velocities. SEM images of eroded samples of 0.69C bainitic steel in Figure 9 reveal various erosion mechanisms. Lower angles and velocities show lip formation with continuous chip scratches and microcracks, whereas higher impact angles and velocities lead to large cracks, pit and crater formation, and embedded alumina fragments. The presence of large craters suggests the embedding and subsequent removal of alumina due to repeated impacts.

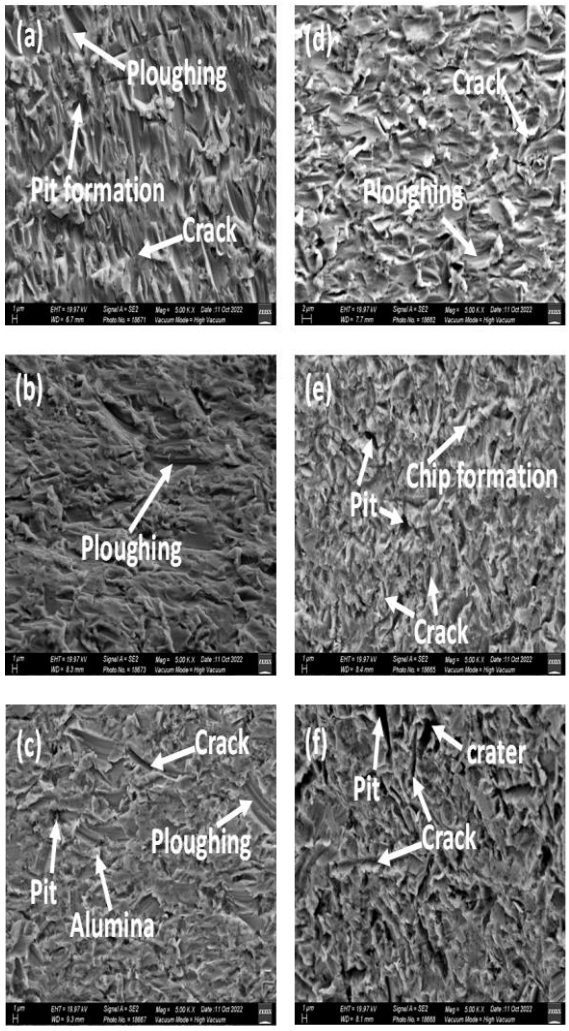

Figure 9: SEM of 0.69 C bainite steel (a) 40 m/s velocity and 15° impact angle (b) 90 m/s velocity and 15° impact angle. (c) 90 m/s and 30° impact angle, and 1.17 C bainite steel (d) 40 m/s velocity and 15° impact angle (e) 60 m/s velocity and 60° impact angle(f)90 m/s velocity and 90° impact angle

5. SEM of 0.69C Bainitic Steel

In the SEM images (Figure 9(a), (b), and (c)), at lower impact angles/lower impact velocities, ploughing and micro-cracks with micro-pitting were observed. At lower impact angles/higher impact velocities, ploughing with large cracks occurred, along with ridge formation after the cutting region. Continuous chips adhering to the material contribute to a lower wear rate. Alumina particles are also embedded at lower angles, and the platelets undergo plastic deformation.

6. SEM of 1.17C Bainitic Steel

In the SEM images (Figure 9 (d), (e), and (f)), lower impact angles/lower impact velocities result in ploughing and microcrack formation. At medium impact angles/medium impact velocities, the surface exhibits scratches, microchipping, and pit formation. Higher impact angles/higher impact velocities lead to the appearance of large cracks, larger pits, and significant craters on the eroded bainitic samples.

7. CONCLUSIONS

This study confirms that the erosion rate on 0.69 C hypo-eutectoid/1.17 C hyper-eutectoid bainitic steel surfaces, subjected to alumina impact, is influenced by impinging velocity, erodent impact angle, and the hardness and microstructure of the targeted steels. Erosion behaviour was analyzed using the erosion power law model (E=k*vn), obtaining velocity exponent (n) values. The average velocity exponent (n) was 2.01 for hypo-eutectoid bainitic steel and 2.39 for hyper-eutectoid bainitic steel, indicating their ductile erosive behaviour. For hypo-eutectoid bainitic steel, SSER was maximum at 30° impact angle for all velocities, while for hyper-eutectoid bainitic steel, it was highest at 60° impact angle (40-60 m/s) and 30° impact angle (90 m/s). The SSER of both steels was minimum at 90° impact angle for all velocities. SEM analysis revealed various erosion mechanisms, including ploughing, cutting, pit formation, etc. At low-impact angles, ploughing with lip formation was observed, decreasing with increasing hardness. At high impact angles, cutting, crack formation, pit, and crater formation, splashing of materials, and embedding of erodent increased with hardness.

8. ACKNOWLEDGEMENTS

I extend my sincere gratitude to the Department of Mechanical/Metallurgical Engineering at IIT (BHU) Varanasi and my esteemed institution for generously providing essential laboratory facilities crucial to the success of this research. Furthermore, I would like to express my heartfelt appreciation to Dr. Harish C. Barshilia, Chief Scientist and Head of the Surface Engineering Division at CSIR-NAL, Bangalore, for graciously allowing access to their SEM and NHT facilities, along with the support of his technical team at the Surface Engineering Division, CSIR-NAL, Bangalore. Special recognition goes to my M.Tech. students, Mr. Utkarsh Choudhary, Mr. Manish Kumar Sharma, and Mr. Anurag, whose invaluable assistance significantly contributed to the experimentation work.

REFERENCES

[1] Tilly, G.P.: Sand erosion of metals and plastics: A brief review, Wear, 14(4), 241–248 (1969)
[2] Finnie, I.: Some observations on the erosion of ductile metals, Wear 19(1), 81–90 (1972)
[3] Finnie, I., Stevick, G.R., Ridgely, J.R.: The influence of impingement angle on the erosion of ductile metals by angular abrasive particles. Wear 152, 91–98 (1992)
[4] Sundararajan, G., Roy, M.: Solid particle erosion behaviour of metallic materials at room and elevated temperatures. Tribology International 30(5), 339–359 (1997)
[5] Hutchings, I.M., Winter, R.E.: Particle erosion of ductile metals: A mechanism of material removal. Wear 27(1), 121–128 (1974)
[6] Ruff, A.W., Ives, L.K.: Measurement of solid particle velocity in erosive wear, Wear, 35(1) 195–199 (1975)
[7] Ives, L.K., Ruff, A.W.: Erosion: Prevention and Useful Applications. Proceedings of the ASTM Symposium 664 (1978)
[8] Harsha, A.P., Bhaskar, D.K.: Solid particle erosion behaviour of ferrous and non-ferrous materials and correlation of erosion data with erosion models. Mater. Des 29(9), 1745–1754 (2008)
[9] Lynn, R.S., Wong, K.K., Mc, H., Clark, I.: On the particle size effect in slurry erosion, Wear 149, 55–71 (1991)
[10] Misra, A., Finnie, I.: On the size effect in abrasive and erosive wear. Wear 65, 359–373 (1981)
[11] Mc, H., Clark, R.B., Hartwich: A re-examination of the 'particle size effect in slurry erosion. Wear 248, 147–161 (2001)
[12] Samuel, J., Rosenberg: The resistance to wear of carbon steels. Bureau of Standards Journal of Research 348, 419–428
[13] Tilly, G.P.: A two stage mechanism of ductile erosion. Wear 23, 87–96 (1973)
[14] Stevenson, A.N.J., Hutchings, I.M.: Scaling laws for particle velocity in the gas-blast erosion test, Wear 181–183(1), 56–62. (1995)
[15] Desale, G.R., Gandhi, B.K., Jain, S.C.: Slurry erosion of ductile materials under normal impact condition. Wear 264, 322–330 (2008)
[16] Molinari, J.F., Ortiz, M.: A study of solid-particle erosion of metallic targets. Int. J. Impact Eng 27, 347–358 (2002)
[17] Mbabazi, J.G., Sheer, T.J., Shandu, R.: A model to predict erosion on mild steel surfaces impacted by boiler fly ash particles. Wear 257, 612–624 (2004)
[18] Akbarzadeh, E., Elsaadawy, E., Sherik, A.M., Spelt, J.K., Papini, M.: The solid particle erosion of 12 metals using magnetite erodent, Wear 282–283, 40–51. (2012)
[19] Torrance, A.A.: An explanation of the hardness differential needed for abrasion. Wear 68, 263–266 (1981)
[20] Desale, G.R., Gandhi, B.K., Jain, S.C.: Slurry erosion of ductile materials under normal impact condition. Wear 264, 322–330 (2008)
[21] Levy, A.V., Yan, J., Patterson, J.: Elevated temperature erosion of steels. Wear 108, 43–60 (1986)
[22] Manish, R., Subramaniyam, M., Sundararajan, G.: Room temperature erosion behaviour of precipitation hardened stainless steel. Tribol Int 25, 271–80 (1992)
[23] Manish, R., Tirupataiah, Y., Sundararajan, G.: Effect of particle shape on the erosion of Cu and its alloys. Mater Sci Eng A 165, 51–63 (1993)
[24] Trilok, S., Tiwari, S.N., Sundararajan, G.: Room temperature erosion behaviour of 304, 316, and 410 stainless steel. Wear 145, 77–100 (1991)

[25] Reddy, A.V., Sundararajan, G., Sivakumar, R., Rao, R., P: Correlation between erosion behaviour and stacking fault energy in copper alloys. Acta metal 32, 1305–1321 (1984)
[26] Edington, J.W., Wright, I.G.: Study of particle erosion damage in Haynes stelite 6B, I: scanning electron microscopy of eroded surfaces. Wear 48, 131–175 (1978)
[27] Edington, J.W., Wright, I.G.: Study of particle erosion damage in Haynes stelite 6B, II: scanning electron microscopy of eroded surfaces. Wear 48, 144–55 (1978)
[28] Ives, L.K., Ruff, A.W.: Electron microscopy study of erosion damage in copper, in erosion: prevention and useful applications. ASTM 664, 5–35
[29] Ruff, A.W., Wiederhorn, S.M.: Erosion by solid particle impact. Treat Mater Sci Technol 16, 69–126 (1979)
[30] Kosel, T.H., Scattergood, R.O., Turner, A.: An electron microscope study of erosive wear. Proceedings of international conference on wear of material, ASME pp. 192–204 (1979)
[31] Kosel, T.H., Turner, A., Scattergood, R.O.: Effects of particle size and shape on erosive wear mechanisms, in corrosion-erosion behaviour of materials. TMSAIME, 146–61 (1980)
[32] Islam, M. A., Alam, T., Farhat, Z. N., Mohamed, A., & Alfantazi, A.: Effect of micro-structure on the erosion behaviour of carbon steel. Wear, 332, 1080-1089 (2015)
[33] Hussain, A. A., Wesley, S.B., Goyal, H. S., and Harsha, A.P.: Investigations on solid particle erosion behaviour of ferritic steels, austenitic steel and low carbon steel and correlation of erosion data with erosion model. Proc IMechE Part J:J Engineering Tribology, 227(3) 234–245 (2012)
[34] DUCOM Manual: The Ducom TR–471-400 air jet erosion test rig manual.